The International Journal of Advanced Manufacturing Technology
https://doi.org/10.1007/s00170-024-13730-5

ORIGINAL ARTICLE

Wear and oxidation behavior of Ti-7Al-1Mo/TiN composites fabricated via spark plasma sintering

Samson Olaitan Jeje[1] · **Mxolisi Brendon Shongwe**[1]

Received: 6 January 2024 / Accepted: 30 April 2024
© The Author(s) 2024

Abstract
The research on the alloys of titanium (Ti) has been extensive due to the need for materials with remarkable resistance to oxidation and wear in demanding applications including the automotive, aerospace, and marine sectors. Even though they have excellent qualities, they frequently require improvements due to the harsh tribological environments they encounter. This study focuses on the ternary alloy of titanium-aluminum-molybdenum (Ti-7Al-1Mo) and its composite (Ti-7Al-1Mo/titanium nitride (TiN)). Utilizing spark plasma sintering (SPS) method, we fabricated these materials with varying TiN weight percentages (1, 3, 5, and 7 wt.%). The microstructural analysis revealed a transition from lath-like morphology to a bimodal structure as TiN content increased. The presence of intermediate Ti_2N phases and hard TiN within the α-Ti matrix was confirmed. Wear tests indicated improved wear resistance in composites, especially at higher TiN fractions, while oxidation resistance increased with TiN content. This research demonstrates the potential of Ti–Al-Mo/TiN composites in high-performance applications, highlighting the nuanced relationship between TiN reinforcement, microstructural evolution, mechanical, and oxidation properties.

Keywords Spark plasma sintering · Titanium matrix composite · Nano-TiN · Wear · Oxidation

1 Introduction

The usage of Ti and its alloy components in automobile, aerospace, petrochemical, and marine applications is attributed to admirable characteristics such as superior strength-to-weight ratio, excellent oxidation, and corrosion resistance [1–4]. The conditions that tribological components are subjected to during service are severe whereby the mechanical properties, wear resistance, and oxidation resistance of Ti and its alloy are not sufficiently good [5]. In applications such as bearings, gear systems, and braking systems, there is a crucial need for materials with excellent wear and oxidation resistance. Ti and its alloys have poor work hardening capability, low surface hardness, and oxide protection [5–8]. Hence, it is essential to study and find the appropriate means to enhance the tribological, oxidative, and mechanical properties of Ti and its alloys.

Reinforcement of Ti and its alloys with ceramics in fabricating a titanium matrix composite (TMC) has been an efficient method of improving its hardness, wear resistance, and thermal stability [9–12]. The strengthening mechanism is a result of factors like dislocation movement hindrance and matrix/reinforcement load transfer [13–15]. There have been positive reviews on reinforcing Ti and its alloy with ceramics like TiN, TiCN, TiC, TiB, TiB_2, ZrO_2, Al_2O_3, Si_3N_4, and SiC [15]. The attention placed on transition-metal nitride (TiN) is a result of the outstanding properties it exhibits. These properties include high hardness, high fracture toughness, excellent thermal and chemical stability, resistance to oxidation, and corrosion [16, 17]. TiN has good thermodynamic stability in the Ti matrix [18] which ensures strong interface bonding, hence offering strength and discouraging reinforcement pull-out during sliding.

The fabrication of TMCs with enhanced mechanical properties has been accomplished by different fabrication techniques in which the powder metallurgy (PM) processing method is established as being effective [2, 15, 19]. In the past decades till recent time, it has been proven beyond reasonable doubt that PM has the capability of producing near-net-shaped

✉ Samson Olaitan Jeje
jejesamsonn@gmail.com

[1] Department of Chemical, Metallurgical and Materials Engineering, Faculty of Engineering and Built Environment, Tshwane University of Technology, Pretoria 0001, South Africa

Published online: 16 May 2024

materials with high performance with low cost and high performance [19]. It has been reported that the conventional routes of sintering (hot isostatic pressing and hot pressing) lead to inefficient reinforcement dispersions and poor sinterability which in turn causes impairment to the overall properties of the sintered material [20, 21]. However, spark plasma sintering (SPS) processing technique is found suitable for the consolidation of TMC due to a direct current of high-intensity and uniaxial pressure simultaneous application which ensures shorter sintering time, relatively low sintering temperature, higher sintered compact relative density, and the limitation of grain growth [2, 15, 22]. Falodun et al. [23] and Kganakga et al. [24] recently worked on reinforcing Ti matrix with TiN nanoceramic via SPS technique. All authors established enhancement in the tribological and mechanical properties of the reinforced Ti matrix. Abe et al. [25] also worked on reinforcing Ti matrix with several refractory nitrides, these include aluminium nitride (AlN), hexagonal boron nitride (h-BN), and titanium nitride (TiN). TiN shows the best resistance against oxidation. Table 1 shows the properties that make TiN a sought-after nanoceramic reinforcement. This work explores the wear and oxidation properties of Ti-7Al-1Mo/TiN composite with different weight percentages of nano-TiN (0, 1, 3, 5, and 7 wt.%) fabricated via SPS technique.

2 Experimental procedures

2.1 Feedstock powders

The mixed powder of T-7Al-1Mo (wt.%) matrix was made using Grade 1 Cp-Ti, Al, and Mo. The reinforcing powder was TiN. Table 2 displays the specific information regarding the powders in their initial form. Five samples of a powder combination based on Ti-7Al-1Mo were produced, and each one had TiN reinforcements with weight percentages of 0, 1, 3, 5, and 7. The T2F Turbula mixer was operated for a duration of 8 h at 49 rpm rotational speed to homogenize the powder in a dry environment. AJOEL JSM-6010 PLUS/LA scanning electron microscope (SEM) was utilized to examine the starting and blended powders. An X-ray diffractometer model PW1710 made by Philips (Cu_Kα radiation at 45 kV/25 mA, 2θ range = 20–100°, $\lambda = 0.154$ nm, count time = 1 s aimed at 0.0167° step) was utilized to perform phase analysis.

2.2 SPS process

By the utilization of HHPD-25 FCT field-assisted sintering machine, the consolidation of the as-mixed powder was successfully achieved. The powder was placed between the upper and lower punches of a graphite die. The pressure within the sintering chamber was adjusted to 10 torr. A pyrometer was used to monitor the temperature during sintering, which was set at 1000 °C with 10 min holding time and a sintering rate of 100 °C per minute. In addition, 50 MPa pressure was employed prior to the start of the cycle (heating). Sandblasting was utilized to eliminate any remaining graphite contamination from the sintered compacts after the sintering process completion. Following that, the compacted samples were prepared for investigation through the application of standard metallographic techniques [15].

Table 1 Properties of TiN

Property	Value/description
Hardness	13.5–19.7 GPa [26]
Fracture toughness	2–6 MPa$\sqrt{m}$ [27, 28]
Melting point	2950 °C
Thermal stability	Excellent [29]
Chemical stability	Resistant to oxidation and corrosion [30]
Thermodynamic stability	Stable in titanium matrix, ensuring strong interface bonding [30]
Resistance	High resistance to wear, abrasion, and erosion [31]

Table 2 As-received powder details

Powder	Supplied by	Purity in %	Size in μm
CP-Ti (grade 1)	TLS Technik GmbH & Co. Germany	99.8	1–25
Al	TLS Technik GmbH & Co. Germany	99.5	1–25
Mo	CERAC, Inc. USA	99.9	1–3
TiN	Nanostructured & Amorphous Material Inc. Texas USA	97	0.02

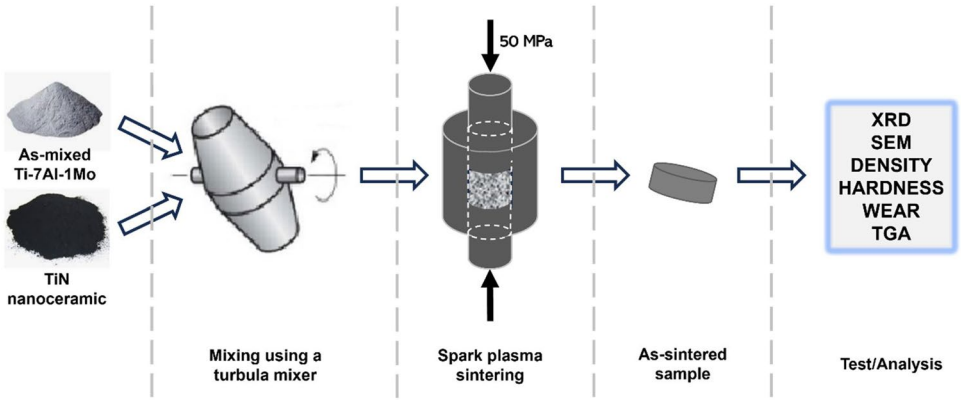

Fig. 1 Schematics of the experimental setup

2.3 Sintered sample characterization

The identification of phases was assessed using an X-ray diffractometer (PW1710 Philips) at Cu_Kα radiation of 45 kV/ 25 mA, 2θ range of 20–100°, λ of 0.154 nm, and count time of 1 s for 0.0167° step. Microstructural study of the sintered samples was done using JOEL JSM-6010 PLUS/LA scanning electron microscope (SEM). The sintered sample's bulk density was recorded using the average of five (5) measurements obtained by using the Archimedes method. The Vicker's hardness value of each sintered sample was recorded from the average of ten indentations achieved by using FUTURE-TECH FM 800 Vicker's hardness tester was set to a holding time of 15 s and load 1 Kgf.

The wear tests without the presence of any lubrication were conducted on the sintered samples using a reciprocating wear drive on a MFT- 5000 RTec universal tribometer. The counterface ball rubbing against the wear specimen was a 6.35-mm diameter alloy steel grade. The wear test was performed at ambient temperature for 1200 s at a length of 3 mm and speed of 4 mm s^{-1}. Each test was conducted at loads of 15, 25, and 35 N for each wear test specimen. To guarantee repeatability, a specific set of conditions was replicated three times. Additionally, the tribometer setup was monitored, the coefficient of friction (COF) was recorded, and the wear rate was computed. The JOEL JSM-6010 SEM was employed to examine the surface morphology that had undergone wear. The ASTM G133-05 (2010) specifications [32] were used to prepare the wear test specimens. Acetone was used to wipe the surface of the ball and test specimens before the wear test to avoid the presence of solid contaminants. Utilizing a thermal gravimetric analyzer (TGA), the oxidation behavior of the created composites was examined. The experiments were conducted within a temperature range of 40 to 800 °C, 10 °C/min heating rate, using high-purity air supplied at a 20 mL/min flow rate. During exposure at the designated temperature range, a Cahn C2000 microbalance reliably recorded the change in mass.

Figure 1 shows the representation of the experimental setup schematics.

3 Results and discussion

3.1 XRD analyses

Figure 2 displays the XRD diffractogram of all the sintered samples, which were examined using X'Pert Highscore Plus Software. The α-Ti (hcp) phase is the major peak found in the fabricated Ti-7Al-1Mo alloy XRD patterns with a β-Ti phase peak found at 38.49° 2Theta angle. However, aside from the α-Ti (hcp) phase major peaks found in the sintered composites (Ti-7Al-1Mo/yTiN, $y=1,3,5$, and 7) pattern, the presence of TiN phase peaks was observed with the evolution of intermediate Ti_2N phase peaks due to the incorporation of TiN nanoceramic reinforcement.

3.2 SEM analyses

Figure 3a–e shows the micrographs of the parallel cross-sections of sintered Ti-7Al-1Mo samples with different wt.% (0–7) of TiN reinforcement, to the pressure applied during sintering. Figure 3a displays a microstructure that is non-porous and has a lamellar lath-like appearance of

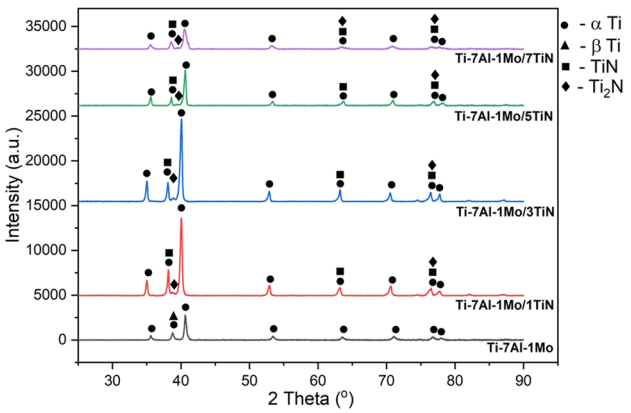

Fig. 2 Sintered compacts' XRD diffractograms

Ti-7Al-1Mo sintered alloy. The morphology is made up of primary α phase (dark contrast), secondary α^{l} phase (light contrast), and β phase (basketweave bright spot contrast at the grain boundary). This conforms to the XRD diffractogram (Fig. 2). Figure 3b–e illustrates the evolution of bimodal structure for the sintered composites and the lath-like morphology was observed to disappear gradually as the reinforcement (TiN nanoceramic) weight percentage increases from 1 to 7. As the TiN content increases, more TiN particles are dispersed throughout the matrix. These particles promote the nucleation of new grains, leading to a finer microstructure. This can disrupt the formation of the typical lamellar structure. Instead, the matrix evolves towards a bimodal distribution of grain sizes or phases, where the influence of TiN becomes dominant at higher weight percentages. The presence of pores in the sintered compacts as the reinforcement increases also indicates a reduction in the relative density. While pores can potentially compromise certain properties, their impact is being mitigated/offset by the positive effects of TiN reinforcement. The mechanical reinforcement provided by TiN nanoparticles can counteract the detrimental effects of pores, leading to an overall improvement in properties such as hardness, wear resistance, and potentially oxidation resistance. The presence of TiN particles as hard inclusions hinders the movement of dislocations in the matrix. Hence, TiN particles help to nucleate new grains during the cooling down of the sample, which can further strengthen the sintered samples.

3.3 Relative density and hardness

Table 3 presents the relative density and hardness values of every sample that underwent spark plasma sintering. The alloy Ti-7Al-1Mo possesses a 99.68% relative density. The study found that as the amount of reinforcement increased, the sintered composites' relative density decreased. Ti-7Al-1Mo composites with reinforcement of 1, 3, 5, and 7 wt.% of TiN have values of 99.55%, 98.54%, 98.22%, and 97.91%, respectively. This conforms with the pores found in the composites' microstructures (Fig. 3). The higher densification observed in this work can be attributed to the sintering temperature surpassing the β transus temperature. Due to the effectiveness of the particle diffusion of Ti–Al and Ti–Ti in the β phase region in comparison to the α phase region due to a higher diffusion coefficient [33], the addition of reinforcement to Ti-7Al-1Mo ternary alloy led to the enhancement of the value of hardness from 352 ± 17 to 370 ± 15 and 549 ± 22 as the reinforcement varied from 1 to 7 wt.%, respectively.

Table 3 Relative density and hardness values of sintered compacts

Sample	Relative density (%)	Hardness ($HV_{1.0}$)
Ti-7Al-1Mo	99.68	352 ± 17
Ti-7Al-1Mo/1TiN	99.55	370 ± 15
Ti-7Al-1Mo/3TiN	98.54	426 ± 24
Ti-7Al-1Mo/5TiN	98.22	453 ± 21
Ti-7Al-1Mo/7TiN	97.91	549 ± 22

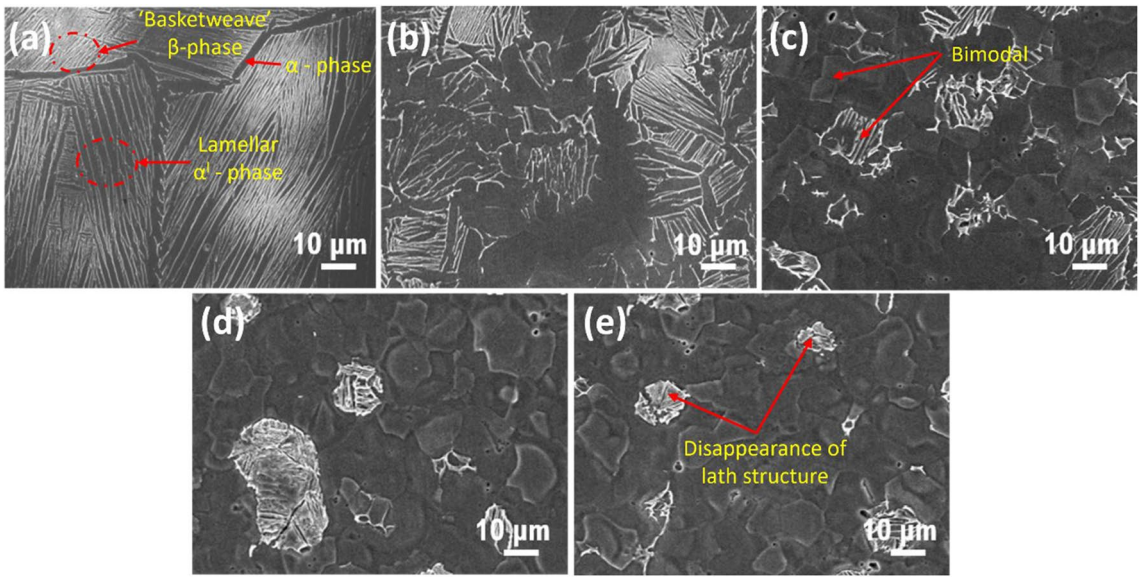

Fig. 3 Sintered compacts' morphology (**a**) Ti-7Al-1Mo (**b-e**) Ti-7Al-1Mo reinforced with 1, 3, 5, and 7 wt.% of TiN, respectively

3.4 Wear behavior of the composites

Ti-7Al-1Mo and Ti-7Al-1Mo/yTiN compacts that were sintered at 1000 °C underwent a tribological test. Ti-7Al-1Mo/yTiN composites' microstructures (Figs. 3b–e) show the existence of pores that differ from the sintered Ti-7Al-1Mo compact's microstructures (Fig. 3a) devoid of visible pores. This is consistent with the relative density values. Consequently, holes could potentially affect their tribological properties. All of the examined compacts had wear scars that could be seen with the unaided eye following the test, indicating the presence of measurable wear "activity."

3.4.1 Frictional behavior

For Ti-7Al-1Mo/TiN sintered compacts, the COF patterns are displayed as they vary with sliding time throughout a duration of 1200 s in Fig. 4a–c correspondingly, on a typical 15 N, 25 N, and 35 N load. Ti-7Al-1Mo/yTiN composites exhibit a lower COF than the compacts of Ti-7Al-1Mo, as shown by the graphs for all applied loads. Similar trends can be seen in the plots, where the COF profile decreases with increasing TiN content. The COF of Ti-7Al-1Mo fluctuates from 0.38 to 0.41 at all normal loads, while the COF of Ti-7Al-1Mo reinforced with nanoceramic varies from 0.25 to 0.34. Reinforcing the compact with nano-TiN resulted in a decrease in its coefficient of friction (COF) values, indicating that the reinforced composites' wear qualities had improved. This was consistent with the evaluated samples' wear volume loss values. Similarly, Obadele et al. [34] and Falodun et al. [23] showed a decrease in COF as a result of ceramic reinforcements.

At the normal load of 35 N, there existed a noticeable decrease in Ti-7Al-1Mo/7TiN COF (Fig. 4c), which was noted at 200 s sliding period. The explanation can be linked to the conversion of a two to three-body abrasion process, where the obtained debris from the wear activity acts as an abrasive between the wear track of the composites and the alloyed steel ball. It is anticipated that the particles of this hard debris that has been accumulated will roll and slide, operating as a tribo-layer or being lodged in the worn surface grooves [35, 36]. Ti-7Al-1Mo/7TiN has the best wear qualities because of the lubricating property of the tribo-layer, which lowers the COF. As can be observed in Figs. 4 and 5, this led the Ti-7Al-1Mo/7TiN composite to produce 0.25 average COF value, which was lower compared to the 0.34 to 0.35 range that was observed for other composites.

The values of the steady-state COF (average) at various normal loads for the compacts under investigation are displayed in Fig. 5. For every sample, it was discovered that the average steady-state COF decreased with an upward trend in normal force. The wear debris of the hard oxidized Ti and Al are responsible for the study's observed decrease in average COF with increasing normal load [35]. Sharma and Sehgal [37] also observed a general decrease in Ti-6Al-4 V COF with increasing normal load in the findings, and they

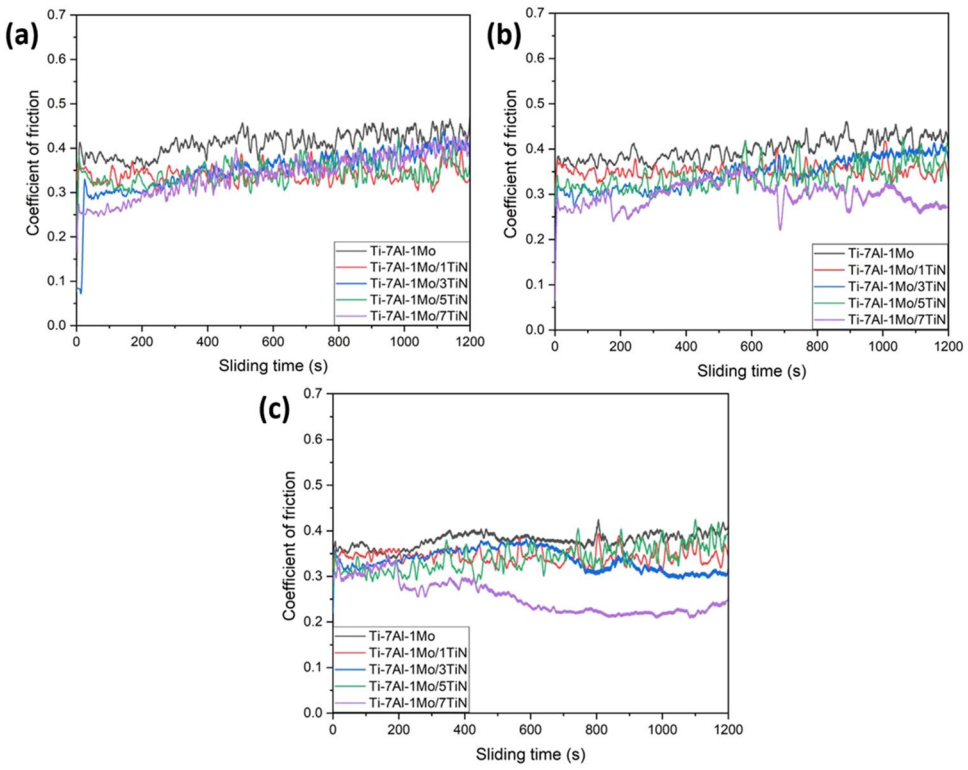

Fig. 4 COF patterns of sintered samples under **a** 15 N, **b** 25 N, and **c** 35 N applied normal loads

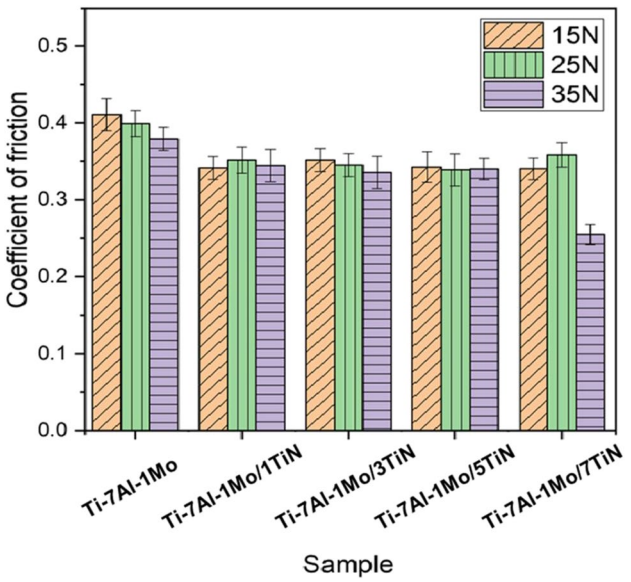

Fig. 5 Sintered compacts' average COF values

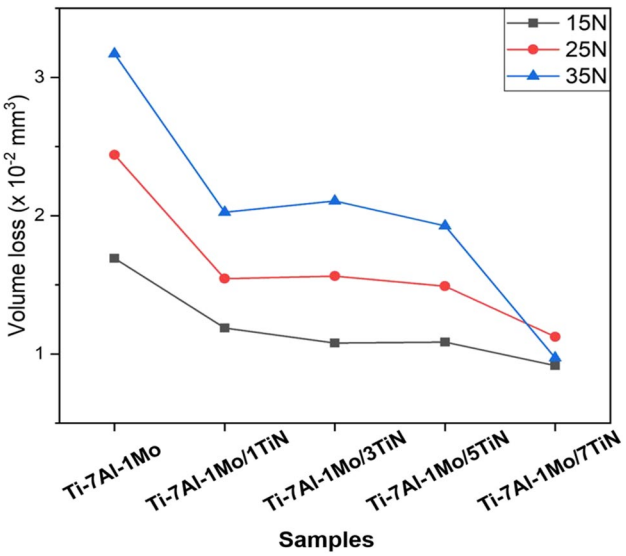

Fig. 6 Sintered compacts' wear volume loss

attributed the decrease to the limited thermal conductivity of the alloy and frictional heating. While the differences in the average coefficient of friction (COF) of the Ti-7Al-1Mo/TiN composites may appear less significant with increasing TiN content, a closer examination of the COF patterns in Fig. 4 reveals distinct differences, particularly at the early stages of wear analysis where the COF values drop with increase in wt.% of TiN. Furthermore, at higher loads of 25 N and 35 N, the distinction in the drop in the COF values for Ti-7Al-1Mo/7TiN composite can be observed from the patterns. The observed drop in COF content during initial sliding periods can be attributed to evolving wear mechanisms and the formation of tribo-layers or oxide plateaus where the effect of change in TiN wt. % was significant. As the sliding time increases, the dispersion and interaction of TiN nanoparticles within the matrix optimize the lubricating and reinforcing effects, stabilizing the wear behavior of the composites, and leading to consistent frictional performance.

3.4.2 Wear volume and wear rate

Figure 6 illustrates the variations in the ternary alloy and composites' wear volume loss under various applied normal loads. Ti-7Al-1Mo ternary alloy was shown to possess the greatest amount of wear volume loss under all normal loads. In general, it was discovered that the wear volume loss for all composites tested rose as the load increased for all test loads. This is consistent with the Wear fundamental laws [1, 38]. In comparison to the Ti-7Al-1Mo compact, composites of this alloy with nano-TiN reinforcement exhibit the least value volume loss. However, as the reinforcement (TiN) content was raised from 1 to 7 wt.%, the composites' wear volume loss decreased. This is explained by the much higher microhardness values of the Ti composites (Table 3) and their resistance to easy deformation under the applied stresses [39, 40]. This is consistent with Archard's law [41], where the wear volume loss of a material and the hardness value are inversely related. According to Liu et al. [42], this suggests that materials with greater hardness values are the source of the lesser volume loss.

As the weight percentage of TiN increases, wear resistance is improved because of the matrix's TiN dispersion increasing and the reinforcement's strong adherence to the matrix [43, 44]. As the wt.% of TiN increases, the dispersion of TiN nanoparticles within the matrix becomes more uniform and dense. This increased dispersion facilitates better interfacial bonding and mechanical interlocking between the TiN particles and the matrix phases, leading to stronger adherence. The improved interfacial bonding at higher TiN percentages promotes more effective load transfer and stress distribution during wear, ultimately contributing to the enhanced wear resistance of the Ti-7Al-1Mo/TiN composite material. Therefore, while some level of adherence existed at lower TiN content, the benefits of increased TiN dispersion and interfacial bonding become more pronounced as the TiN content rises, positively impacting wear resistance. This outcome is consistent with the studies of Balla et al. [45] and Falodun et al. [46] where it was found that adding nano-TiN reinforcement to Ti-alloy (Ti6Al4V) increased its resistance to wear.

Figure 7 displays the relationship among sintered compacts' specific wear rate, composition, and test load. The samples' specific wear rate decreased when both the TiN weight percentage and the normal sliding load increased.

At 15, 25, and 35 N normal loads, Ti-7Al-1Mo ternary alloy recorded wear rates of 2.35×10^{-4}, 2.03×10^{-4}, and 1.89×10^{-4} $mm^3/(Nm)$, respectively. For the Ti-7Al-1Mo/7TiN composite, 1.27×10^{-4}, 0.93×10^{-4}, and 0.57×10^{-4} $mm^3/(Nm)$ were recorded for the wear rates respectively. When compared to Ti-7Al-1Mo, a drop of roughly 45 to 70% in the specific wear rate for Ti-7Al-1Mo/7TiN was observed. Additionally, an increase in surface roughness may have resulted in the presence of hard TiN and Ti_2N phases as well as the wear debris of oxidized Ti that was ejected onto the surface and presented itself as a tribo-film (i.e., titanium oxide plateau) that reduced friction, which serves as the basis why with increasing load, the specific wear rate was decreasing [35].

3.4.3 Wear scar morphology

Under 15 N, 25 N, and 35 N applied stress, the worn surfaces micrographs (SEM) of the composites and the ternary alloy are displayed in Fig. 8. The magnification of all the SEM micrographs is the same. Comparing the worn-out Ti-7Al-1Mo surfaces (Fig. 8a–c) to the matching Ti-7Al-1Mo/TiN composites at each test load, the former exhibits parallel and deeper grooves in the sliding direction. This may be due to Ti-7Al-1Mo's comparatively low hardness value, which resulted in inadequate abrasion resistance. Falodun et al. [23] reported that the inadequate protection provided by the surface oxide and insufficient resistance to plastic shearing due to high friction-generated flash temperature are the causes of the relatively low level of the $Ti-6Al-4\,V$ wear resistance exhibited in contrast to Ti-6Al-4 V/TiN composites.

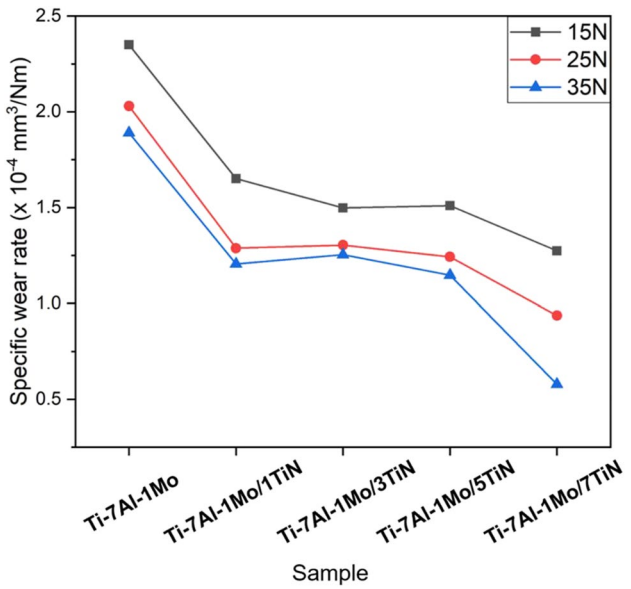

Fig. 7 Sintered compacts' specific wear rate

Furthermore, the compact without TiN reinforcement's higher adhesion tendencies may be due to its relatively high ductility when compared to the produced reinforced composites [15]. Deep abrasive groves are the result of the worn area becoming work-hardened.

The worn micrographs of Ti-7Al-1Mo, which have weight percentages of 5 and 7 nano-TiN (Fig. 8j–l and m–o, correspondingly), show that the wear scar's breadth has decreased, suggesting that the counter-face alloy steel ball has penetrated less deeply. The degree of wear is anticipated to be influenced by surface hardness. The maximum hardness value as observed for Ti-7Al-1Mo/7TiN results in less surface abrasion penetration. As a result, less material was removed from the surface by the "plowing" activity, which led to less plastic flow being seen. This is explained by the growth of the Ti_2N intermediate phase and the large percentage of the TiN hard phase, which increase the resistance of the material to plastic deformation. The wear volume loss displayed in Fig. 6 is consistent with these findings.

3.5 Thermogravimetric analysis (TGA)

The oxidation behavior of the studied samples as measured by weight gain is displayed in Fig. 9 corresponding to temperature rise from 40 to 800 °C. The degree of oxidation varied throughout the examined samples. As the temperature rises, the pattern exhibits a single parabolic kinetic pattern and mass increment. This suggests a diffusion-controlled process [47]. A substantial mass change was noted in the Ti-7Al-Mo ternary alloy curve starting at a temperature of roughly 600 °C. This implies that there are differences in the mechanism controlling the oxidation process occurring below and above 600 °C. Due to Ti's affinity for O, Ti exhibits a propensity to undergo oxidation, resulting in the formation of a protective oxide layer primarily composed of titanium dioxide (TiO_2) when subjected to temperatures exceeding 600 °C. To shield the tested compact's surface from additional oxidative environment attack, the protective layer (TiO_2) gets thicker. Defective oxide structure development after crystallization promotes the diffusion pathways of Ti ions and oxygen. Consequently, when the temperature rises, oxidation has a tendency to occur [48]. The protective barrier is extremely thin between 600 and approximately 650 °C, and the electric field created between the outer (TiO_2/air) and inner (Ti/TiO_2) interfaces controls the movement of matter. As a result, the movement of ionic species is predominant and causes oxidation kinetics, which raises the oxide layer in accordance with the inverse logarithmic rule. Diffusion takes over migration above 650 °C, and it subsequently regulates the oxidation kinetics [49]. Hence, at a temperature close to 650 °C, an exponential rise in weight gain was noted.

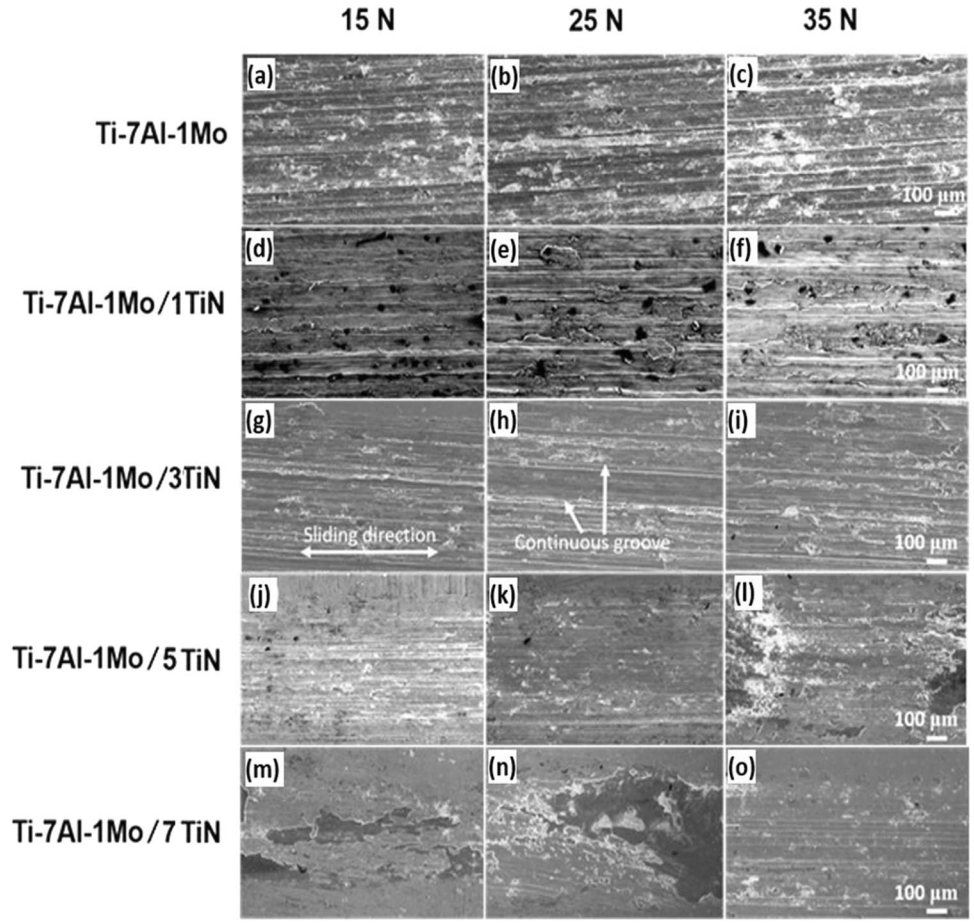

Fig. 8 Sintered compacts' SEM images of worn surface

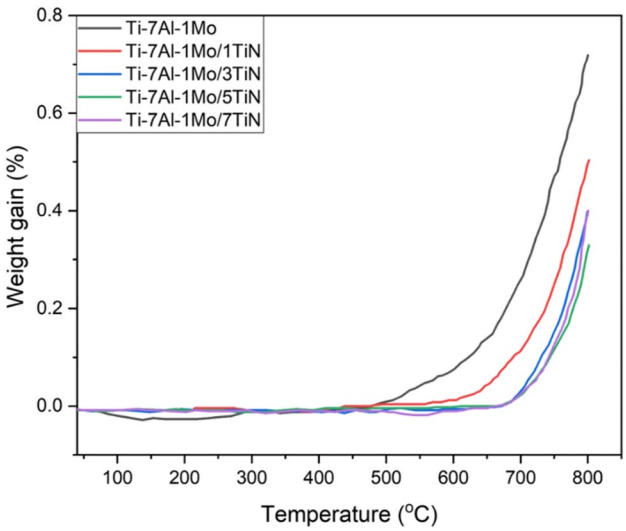

Fig. 9 TGA of sintered samples

Ti-7Al-1Mo/yTiN composites showed a similar oxidation mechanism. Nonetheless, for TiN reinforcement of 3, 5, and 7 wt.%, a notable increase in weight gain was seen at a higher temperature of roughly 700 °C. This suggests that the thermal stability and oxidation resistance of Ti-7Al-1Mo ternary alloy were enhanced when reinforced with nanoceramic TiN. This is explained by the addition of an intermediate Ti2N phase, which aids in further oxidation resistance, and a highly thermally stable TiN phase.

Based on the oxidation test, the overall weight gain seen for the examined samples is displayed in Fig. 10. Ti-7Al-1Mo/5TiN has the least weight gain of roughly 0.33%, indicating that the oxidative property of this alloy has improved with the addition of reinforcement, according to the trend. This represents approximately a 54% decrease in weight gain relative to Ti-7Al-1Mo's 0.72% weight gain.

4 Conclusion

The SPS method was successfully employed to produce the ternary alloy of Ti–Al-Mo and the Ti–Al-Mo/yTiN ($y = 1$, 3, 5, and 7) composites. All of the sintered compacts' oxidative characteristics and wear were examined. The obtained results are as follows:

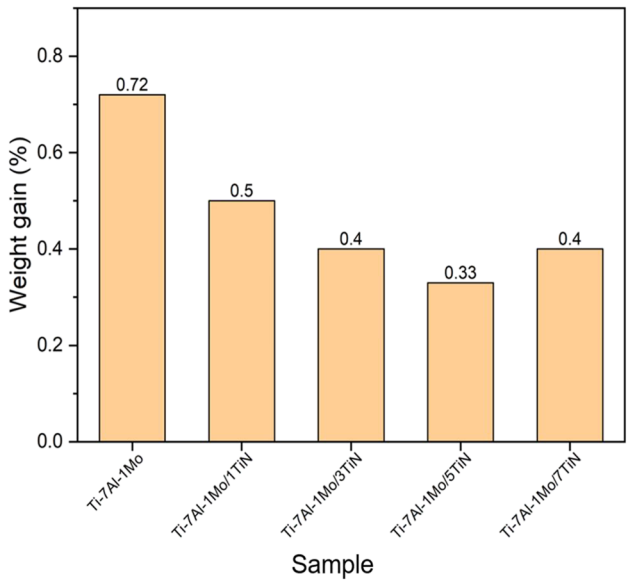

Fig. 10 Weight gain for tested samples after the oxidation test

- Increment in the wt.% (from 1 to 7) of TiN reinforcement, resulted in a decrease in the composites' relative density.
- The ternary alloy Ti-7Al-1Mo exhibits a Widmanstatten lath-like shape that is non-porous, primarily composed of α lamellar phases with a small amount of β "basketweave" phase maintained at the grain boundaries. When the weight percentage of TiN increased, the lath-like shape vanished and a bimodal structure evolved.
- Hard TiN and intermediate Ti_2N phases evolved inside the α-Ti matrix for TiN-reinforced Ti-7Al-1Mo.
- For all examined samples, as the applied load increased, the wear volume loss decreased; however, the specific wear rate experienced an opposite trend.
- An increase from 1 to 7% in the weight percentage of the reinforcement (TiN) led to improved wear resistance of the composites over the Ti-7Al-1Mo ternary alloy.
- The oxidation resistance of the composites is further enhanced by an increase in the weight percentage of TiN. Composite with 5 wt.% of TiN reinforcement gave the best oxidative properties.

Author contribution Samson Olaitan Jeje: conceptualization, methodology, investigation, formal analysis, and writing—original draft preparation. Mxolisi Brendon Shongwe: supervision, formal analysis, and writing—review and editing.

Funding Open access funding provided by Tshwane University of Technology. This work is based on the research supported in part by the National Research Foundation of South Africa (Ref number: CSUR230430100268). The authors acknowledge the financial support for this research by the Faculty of Engineering and Built Environment, Tshwane University of Technology, and the Department of Chemical, Metallurgical and Materials Engineering of the Tshwane University of Technology, Pretoria, South Africa.

Data availability The data that support the findings of this study are available from the corresponding author upon reasonable request.

Code availability Not applicable.

Declarations

Ethics approval Not applicable.

Consent to participate Not applicable.

Competing interests The authors declare no competing interests.

Open Access This article is licensed under a Creative Commons Attribution 4.0 International License, which permits use, sharing, adaptation, distribution and reproduction in any medium or format, as long as you give appropriate credit to the original author(s) and the source, provide a link to the Creative Commons licence, and indicate if changes were made. The images or other third party material in this article are included in the article's Creative Commons licence, unless indicated otherwise in a credit line to the material. If material is not included in the article's Creative Commons licence and your intended use is not permitted by statutory regulation or exceeds the permitted use, you will need to obtain permission directly from the copyright holder. To view a copy of this licence, visit http://creativecommons.org/licenses/by/4.0/.

References

1. Jeje SO, Shongwe MB, Ogunmuyiwa EN, Rominiyi AL, Olubambi PA (2020) Microstructure, Hardness, and Wear Assessment of Spark-Plasma-Sintered Ti-x Al-1Mo Alloy. Metall Mater Trans A 51:4033–4044
2. Rominiyi AL, Shongwe MB, Tshabalala LC, Ogunmuyiwa EN, Jeje SO, Babalola BJ, Olubambi PA (2020) Spark plasma sintering of Ti–Ni–TiCN composites: Microstructural characterization, densification and mechanical properties. J Alloys Compd 848
3. Jeje SO, Shongwe MB, Maledi N, Ogunmuyiwa EN, Tshabalala LC, Babalola BJ, Olubambi PA (2020) Sintering behavior and alloying elements effects on the properties of CP-Titanium sintered using pulsed electric current. Mater Chem Phys 256:123707
4. Jeje SO, Shongwe MB, Rominiyi AL, Babalola BJ, Olubambi PA (2021) Spark plasma sintering behavior of Ti-3Al-1Mo alloy. Mater Today Proc 38:1121–1125
5. Li CZ, Fu BG, Dong TS, Liu JH, Song YJ, Zhao XB, Li GL (2020) Microstructure and dry sliding wear behavior of as-cast TiC p/Ti-1100-0.5 Nb titanium matrix composite at elevated temperatures. China Foundry 17:455–463
6. Alam MO, Haseeb ASMA (2002) Response of Ti–6Al–4V and Ti–24Al–11Nb alloys to dry sliding wear against hardened steel. Tribol Int 35(6):357–362
7. Zhao J, Zhang ZY, Liu SB, Shi K, Bao CL, Ning ZS, Yan P, Wang L, Lou YC (2020) Elimination of misrun and gas hole defects of investment casting TiAl alloy turbocharger based on numerical simulation and experimental study. China Foundry 17(1):29–34

8. De Formanoir C, Brulard A, Vivès S, Martin G, Prima F, Michotte S, Rivière E, Dolimont A, Godet S (2017) A strategy to improve the work-hardening behavior of Ti–6Al–4V parts produced by additive manufacturing. Mater Res Lett 5(3):201–208
9. Tjong SC, Mai YW (2008) Processing-structure-property aspects of particulate-and whisker-reinforced titanium matrix composites. Compos Sci Technol 68(3–4):583–601
10. Tjong SC, Ma ZY (2000) Microstructural and mechanical characteristics of in situ metal matrix composites. Mater Sci Eng R Rep 29(3–4):49–113
11. Ma P, Wei ZJ, Jia YD, Yu ZS, Prashanth KG, Yang SL, Li CG, Huang LX, Eckert J (2017) Mechanism of formation of fibrous eutectic Si and thermal conductivity of SiCp/Al-20Si composites solidified under high pressure. J Alloys Compd 709:329–336
12. Jeje SO, Shongwe MB, Maledi N, Rominiyi AL, Adesina OS, Olubambi PA (2021) Synthesis and characterization of TiN nanoceramic reinforced Ti–7Al–1Mo composite produced by spark plasma sintering. Mater Sci Eng, A 807:140904
13. Zhang Z, Chen DL (2008) Contribution of Orowan strengthening effect in particulate-reinforced metal matrix nanocomposites. Mater Sci Eng A 483:148–152
14. Nardone V, Prewo KJSM (1986) On the strength of discontinuous silicon carbide reinforced aluminum composites. Scr Metall 20(1):43–48
15. Jeje SO, Shongwe MB, Maledi N, Rominiyi AL, Adesina OS, Olubambi PA (2021) Synthesis and characterization of TiN nanoceramic reinforced Ti–7Al–1Mo composite produced by spark plasma sintering. Mater Sci Eng A 807:140904
16. Szutkowska M, Cygan S, Podsiadło M, Laszkiewicz-Łukasik J, CySzutkowska M, Cygan S, Podsiadło M, Laszkiewicz-Łukasik J, Cyboroń J, Kalinka A (2019) Properties of TiC and TiN reinforced alumina–zirconia composites sintered with spark plasma technique. Metals 9(11):1220
17. Guo B, Zhou J, Zhang S, Zhou H, Pu Y, Chen J (2008) Microstructure and tribological properties of in situ synthesized TiN/Ti3Al intermetallic matrix composite coatings on titanium by laser cladding and laser nitriding. Mater Sci Eng A 480(1–2):404–410
18. Srinivasan D, Kulkarni TG, Anand K (2007) Thermal stability and high-temperature wear of Ti–TiN and TiN–CrN nanomultilayer coatings under self-mated conditions. Tribol Int 40(2):266–277
19. Prakash KS, Gopal P, Anburose D, Kavimani V (2018) Mechanical, corrosion and wear characteristics of powder metallurgy processed Ti-6Al-4V/B4C metal matrix composites. Ain Shams Eng J 9(4):1489–1496
20. Mussatto A, Ahad IU, Mousavian RT, Delaure Y, Brabazon D (2021) Advanced production routes for metal matrix composites. Engineering reports 3(5):e12330
21. Kim IY, Choi BJ, Kim YJ, Lee YZ (2011) Friction and wear behavior of titanium matrix (TiB+ TiC) composites. Wear 271(9–10):1962–1965
22. Matizamhuka WR (2016) Spark plasma sintering (SPS)-an advanced sintering technique for structural nanocomposite materials. J South Afr Inst Min Metall 116(12):1171–1180
23. Falodun OE, Obadele BA, Oke SR, Ige OO, Olubambi PA, Lethabane ML, Bhero SW (2018) Influence of spark plasma sintering on microstructure and wear behaviour of Ti-6Al-4V reinforced with nanosized TiN. Trans Nonferrous Metals Soc China 28(1):47–54
24. Kganakga MG, Prieto G, Falodun OE, Tuckart WR, Obadele BA, Ajibola OO, Olubambi PA (2020) Erosion wear behavior of spark plasma-sintered Ti-6Al-4V reinforced with TiN nanoparticles. J South Afr Inst Min Metall 110:3051–3060
25. Abe JO, Popoola API, Popoola OM (2020) Consolidation of Ti6Al4V alloy and refractory nitride nanoparticles by spark plasma sintering method: Microstructure, mechanical, corrosion and oxidation characteristics. Mater Sci Eng A 774:138920
26. Drygas M, Lejda K, Janik JF, Stelmakh S, Palosz B (2022) Novel composite nitride nanoceramics from reaction-mixed nanocrystalline powders in the system aluminum nitride AlN/gallium nitride GaN/titanium nitride TiN (Al: Ga: Ti= 1: 1: 1). Materials 15(6):2200
27. Mofidi HH, Rouhaghdam AS, Ahangarani S, Bozorg M, Azadi M (2014) Fracture toughness of TiN coating as a function of interlayer thickness. Adv Mater Res 829:466–470
28. Bielawski M, Chen K (2011) Computational evaluation of adhesion and mechanical properties of nanolayered erosion-resistant coatings for gas turbines
29. Maja ME, Falodun OE, Obadele BA, Oke SR, Olubambi PA (2018) Nanoindentation studies on TiN nanoceramic reinforced Ti–6Al–4V matrix composite. Ceram Int 44(4):4419–4425
30. Zhao Y, Wu C, Zhou S, Yang J, Li W, Zhang L-C (2021) Selective laser melting of Ti-TiN composites: Formation mechanism and corrosion behaviour in H2SO4/HCl mixed solution. J Alloy Compd 863:158721
31. Prokudina VK (2017) Titanium nitride. In Concise encyclopedia of self-propagating high-temperature synthesis. Elsevier, pp 398–401
32. G133–05(2016) (2016) Standard test method for linearly reciprocating ball-on-flat sliding wear. ASTM International, West Conshohocken, PA, USA
33. Chaudhari R, Bauri R (2014) Microstructure and mechanical properties of titanium processed by spark plasma sintering (SPS). Metallography Microstruct Anal 3(1):30–35
34. Obadele BA, Andrews A, Olubambi PA, Mathew MT, Pityana S (2015) Effect of ZrO2 addition on the dry sliding wear behavior of laser clad Ti6Al4V alloy. Wear 328:295–300
35. Abdelbary A (2014) 2 - Sliding mechanics of polymers. In: Abdelbary A (ed) Wear of polymers and composites. Woodhead Publishing, Oxford, pp 37–66
36. Narayanan TS (2012) Nanocoatings to improve the tribocorrosion performance of materials. Corrosion Protection and Control Using Nanomaterials. pp 167–212
37. Sharma MD, Sehgal R (2012) Dry sliding friction and wear behaviour of titanium alloy (Ti-6Al-4V). Tribol Online 7(2):87–95
38. Wang Z, Zhou Y, Wang H, Li Y, Huang W (2018) Tribocorrosion behavior of Ti-30Zr alloy for dental implants. Mater Lett 218:190–192
39. Feng X, Sui JH, Cai W, Liu AL (2011) Improving wear resistance of TiNi matrix composites reinforced by carbon nanotubes and in situ TiC. Scripta Mater 64(9):824–827
40. Revankar GD, Shetty R, Rao SS, Gaitonde VN (2017) Wear resistance enhancement of titanium alloy (Ti–6Al–4V) by ball burnishing process. J Market Res 6(1):13–32
41. Hutchings I, Shipway P (2017) Tribology: friction and wear of engineering materials. Butterworth-Heinemann
42. Liu B, Liu Y, He X, Tang H, Chen L, Huang B (2007) Preparation and mechanical properties of particulate-reinforced powder metallurgy titanium matrix composites. Metall Mater Trans A 38(11):2825–2831
43. Fu Y, Zhang XC, Sui JF, Tu ST, Xuan FZ, Wang ZD (2015) Microstructure and wear resistance of one-step in-situ synthesized TiN/Al composite coatings on Ti6Al4V alloy by a laser nitriding process. Opt Laser Technol 67:78–85
44. Yen SK, Guo MJ, Zan HZ (2001) Characterization of electrolytic ZrO2 coating on Co–Cr–Mo implant alloys of hip prosthesis. Biomater 22(2):125–133
45. Balla VK, Bhat A, Bose S, Bandyopadhyay A (2012) Laser processed TiN reinforced Ti6Al4V composite coatings. J Mech Behav Biomed Mater 6:9–20
46. Falodun OE, Obadele BA, Oke SR, Maja ME, Olubambi PA (2018) Effect of sintering parameters on densification and microstructural evolution of nano-sized titanium nitride reinforced titanium alloys. J Alloy Compd 736:202–210
47. Ridley MJ, Opila EJ (2021) Thermomechanical and thermochemical stability of HfSiO4 for environmental barrier coating applications. J Am Ceram Soc 104(7):3593–3602

48. Gemelli E, Camargo NHA (2007) Oxidation kinetics of commercially pure titanium. Matéria (Rio de Janeiro) 12:525–531
49. Guleryuz H, Cimenoglu H (2009) Oxidation of Ti–6Al–4V alloy. J Alloys Compd 472(1–2):241–246

Publisher's Note Springer Nature remains neutral with regard to jurisdictional claims in published maps and institutional affiliations.